Spectrum - The Journal of Operational Applications in Defense Areas

Journal homepage: https://spectrum.ita.br

Electronic Warfare and Remote Sensing: Analysis and Development of Optical Sensors

A Laboratory Radiometric Calibration of an Electro-Optical Sensor

Marcus Vinnicius de Q. S. A. Costa[1], Alvaro José Damião[2,3] and Ruy Morgado de Castro[3]

[1]Comando de Preparo (COMPREP), Brasília/DF – Brasil

[2]Instituto Tecnológico de Aeronáutica (ITA), São José dos Campos/SP – Brasil

[3]Instituto de Estudos Avançados (IEAV), São José dos Campos /SP – Brasil

Article Info

Article History:

Received	15 May	2025
Revised	28 June	2025
Accepted	21 July	2025
Available online	23 September	2025

Keywords:

Optical remote sensing

Radiometric calibration

Spectral calibration

E-mail adresses:

marcuscosta@ita.br
alvdamiao@terra.com.br
ruymcastro@gmail.com

Abstract

Remote sensing imaging satellites play a vital role in Intelligence, Surveillance, and Reconnaissance (ISR) missions, as they enable the acquisition of information from virtually any location on the Earth's surface. To ensure the reliability of the provided information, it is essential to calibrate the onboard sensors on these satellites. This paper aims to present a methodology for spectral and radiometric calibration of a Parrot Sequoia camera in laboratory settings. This camera features four monochromatic sensors and one RGB sensor, similar to those onboard orbital platforms. The methodology described employs equipment available at the Laboratory of Radiometry and Characterization of Electro-Optical Sensors (LaRaC) at the Institute for Advanced Studies (IEAv). The paper presents the Spectral Response Functions (SRFs) of the camera sensors, as well as the Radiometric Calibration data. It is worth noting that the proposed methodology can be replicated for any other orbital electro-optical imaging sensor.

I. INTRODUCTION

Remote sensing satellites are key assets employed by the Air Force for Intelligence, Surveillance, and Reconnaissance (ISR) missions [1]. By acquiring images of points of interest on the Earth's surface, their usage significantly enhances the situational awareness of the Armed Forces, supporting decisively in decision-making and operational planning.

For successful operation, the calibration of the onboard sensors is essential to understand their spectral, radiometric, and spatial characteristics. Proper calibration, starting from the pre-launch phase, ensures that users receive reliable data from the system [2].

Radiometric calibration specifically requires an understanding of the relationship between the Digital Numbers (DN) of the pixels in the images generated by the camera's sensor and the radiance reaching that sensor from the imaged surface. To achieve this, the Spectral Response Function (SRF) of the camera must be determined, which describes how the sensor responds to radiation at each wavelength.

This DN-to-radiance relationship should be established early in the sensor development phase, and the calibration procedures must be performed in a laboratory before satellite launch. Developers of an orbital sensor must master this methodology, not relying solely on manufacturer data. This technical knowledge enhances the capability of human resources responsible for satellite operations and leads to better-informed decisions during the acquisition of new systems.

Accordingly, to provide the Brazilian Air Force with the necessary expertise for laboratory radiometric calibration of orbital optical sensors, this paper presents a methodology for the calibration of the Parrot Sequoia camera using equipment from the Laboratory of Radiometry and Characterization of Electro-Optical Sensors (LaRaC), located at the Institute for Advanced Studies (IEAv). Section II presents theoretical aspects of optical sensor calibration. Section III describes the main equipment used during the process. Section IV details the spectral characterization procedure, while Section V outlines the radiometric calibration methodology. Section VI concludes with results and final considerations.

II. OPTICAL SENSOR CALIBRATION

An orbital optical imager is a system with electro-optical sensors, onboard a satellite, capable of receiving radiance (radiative flux per area and solid angle) from the Earth's surface [3]. The most common sensors are multispectral, operating across various bands, typically Blue, Green, Red, and Near Infrared (NIR) [4]. Fig. 1 shows the Spectral Response Functions (SRFs) of four sensors onboard CBERS-4, Landsat-7, and Landsat-8 [2]. In general, SRFs are values ranging from 0 to 1, representing the relative sensitivity of the sensor at each wavelength. It is evident that even when operating in similar bands, their spectral responses differ.

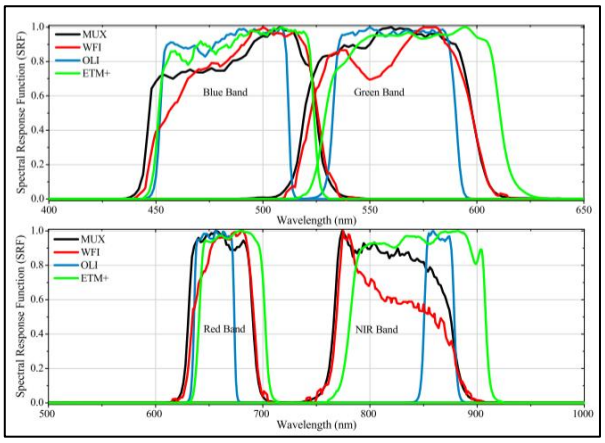

Fig. 1. SRF from four different orbital optical sensors.

When exposed to radiation in their operating bands, the sensor's internal detectors generate electrical signals converted into Digital Numbers (DNs). CCD cameras, which use arrays of detectors, are a common example [4]. Each cell in this array corresponds to a pixel whose DN is proportional to the incident radiation. The resulting image is a composition of all the pixels, where each DN value corresponds to a grayscale intensity defined by the sensor's radiometric resolution.

Radiometric resolution is defined by the number of bits (n). Each detector can generate n binary digits (0 or 1) proportional to the electrical signal, which in turn is proportional to the incident energy. As a result, the received energy can be discretized into up to 2^n digital levels, representing the total number of possible combinations of the n binary digits [4].

From these DN values, it is possible to retrieve radiance values from the surface observed. Typically, manufacturers design sensors so the DN-to-radiance relationship follows a linear function (1) [5].

$$L_i = G_i \cdot ND_i + B_i, \qquad (1)$$

where L_i is the radiance in band i, G_i is the gain coefficient, and B_i is the bias (or offset) coefficient in that band, related to the detector's dark current (response in the absence of radiance) [4].

A sensor calibration consists in determining the G_i and B_i coefficients, which allows to estimate radiance from image DN.

III. EQUIPMENT USED

Due to the unavailability of orbital sensors for the purposes of this study, the calibration procedure employed the Parrot Sequoia camera. Although not designed specifically for orbital applications, this camera was selected for its features that closely resemble those found in optical sensors onboard remote sensing satellites.

Firstly, the spectral characterization, aimed at finding the Spectral Response Function (SRF), a light source combined with a monochromator was used to illuminate the sensor with monochromatic light at specific wavelengths.

Subsequently, an Integrating Sphere equipped with lamps at specific power was employed. The light radiance emitted from the output port of the sphere was measured using the FieldSpec 4 spectroradiometer. The overall calibration procedure is described in Sections IV and V.

A. Parrot Sequoia Camera

The Parrot Sequoia camera was developed for drone-based remote sensing applications in precision agriculture [6]. Although its primary application differs from orbital missions, its technical specifications are comparable, and the calibration process is identical. Fig. 2 illustrates the equipment, and Table I provides an overview of its key specifications.

Fig. 2. Parrot Sequoia camera [7].

TABLE I. PARROT SEQUOIA CAMERA CHARACTERISTICS [6].

Sensor	Wavelength (nm)	Bandwidth (nm)	Max definition	Radiometric Resolution (bits)
Green	550	40		
Red	660	40		
Red Edge (REG)	735	10	1.2 MP	10
Near Infrared (NIR)	790	40		
RGB	-		16 MP	8

The Sequoia's operational bands are similar to those of orbital sensors, except for the absence of a Blue band in its monochromatic set and the inclusion of a Red Edge (REG) band, which is typically not found in orbital sensors. The camera also includes an RGB (red, green and blue) sensor capable of capturing full-color images. Metadata from the camera images indicates an *f-number* of 2.2 for the monochromatic sensors and 2.3 for the RGB sensor. The field of view is 61.9° for the monochromatic sensors and 65.5° for the RGB sensor.

By default, the camera operates in automatic mode, adjusting ISO and exposure time using a called "Sunshine Sensor", which evaluates ambient lighting conditions and sets ISO and exposure time for each shot. However, for the calibration experiments, it was necessary to use manual mode to ensure identical camera settings across all measurements. Manual control was achieved through the camera's Application Programming Interface (API) using the Postman software [8].

B. Monochromator

The Acton SpectraPro-2500i monochromator used in this study features turrets equipped with three interchangeable diffraction gratings, which can be selected according to the selected wavelength range. Upon receiving broadband radiation at its input, the instrument diffracts and spatially separates the light into specific wavelengths.

The output radiation corresponds to the user-selected wavelength, controlled through dedicated software, with an accuracy of ±0.2 nm [9] (Fig. 3).

For this study, the grating optimized for 500 nm was used, as the wavelength range for the experiments was between 400 and 850 nm. The broadband light source used was a 100 W tungsten lamp.

Fig. 3 Acton SpectraPro-2500i monochromator [9].

C. Integrating Sphere

The Labsphere USS-2000 integrating sphere used in this work has a diameter of 500 mm and a 200 mm output port. Its interior is coated with Spectraflect®, a highly diffuse reflective material covering the 250–2400 nm spectral range [10].

The integrating sphere is equipped with four halogen lamps of varying power ratings—A (150 W), B (45 W), C (100 W), and D (45 W). These lamps can be activated in multiple combinations to produce eleven distinct radiance levels. Fig. 4 shows the experimental setup with the FieldSpec 4 spectroradiometer.

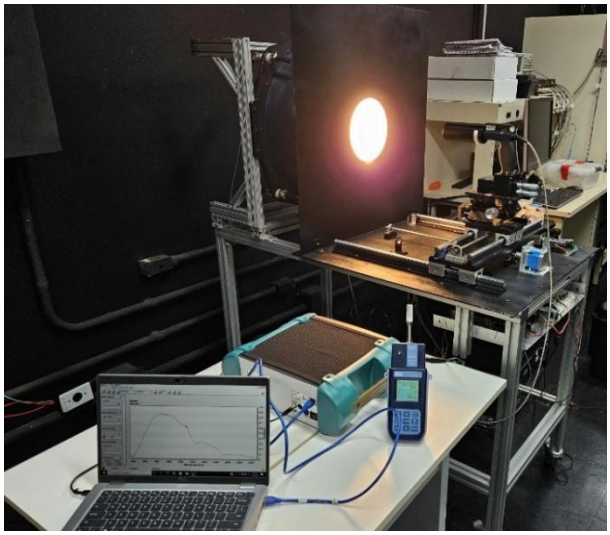

Fig. 4. Experimental setup for radiometric characterization with the FieldSpec 4 spectroradiometer.

D. FieldSpec 4 Spectroradiometer

The FieldSpec 4, as shown in Fig. 4, is a spectroradiometer with fixed optical fibers capable of measuring radiant energy in the 350–2500 nm wavelength range, encompassing the visible, near-infrared, and shortwave infrared regions. It is designed for field-based remote sensing applications and supports spectral acquisitions at intervals as short as 0.2 seconds [11].

IV. Spectral Characterization (Obtaining the SRF)

This initial stage aims to determine the relative sensitivity of the sensor at each wavelength. The result is the Spectral Response Function (SRF), which is also necessary for the next stage: radiometric calibration.

Fig. 5 schematically presents the data collection and analysis process for this step. The equipment used for data acquisition—namely the Parrot Sequoia camera and the reference detector, both illuminated by radiation passing through the monochromator—is shown in light orange. The red numbers indicate the data generated at each phase, which will be used in both this step and the subsequent calibration. The blue items represent the results of data processing. The variable $DN_{cam}(\lambda)$ corresponds to the digital numbers produced by the camera at each wavelength, $V_{det}(\lambda)$ refers to the voltage output by the reference detector, and the standard deviations are denoted by σ (λ). The function $SRF_{det}(\lambda)$ is the known spectral response of the reference detector, and $SRF_{cam}(\lambda)$ is the SRF of the camera, which is the main target of this stage. After normalization, this function becomes $SRF_{norm}(\lambda)$.

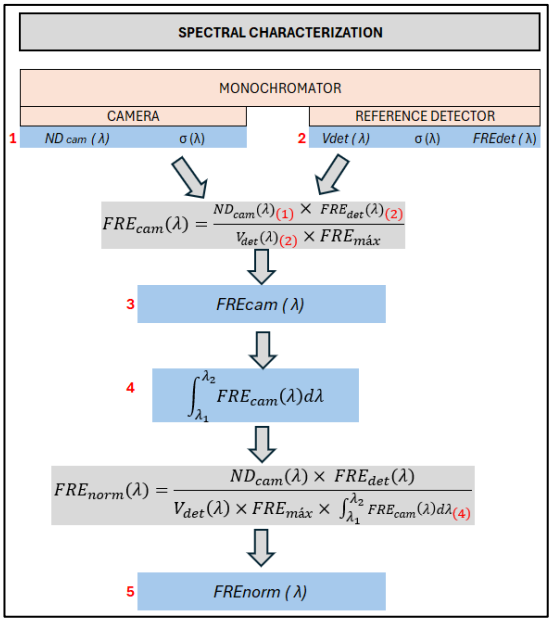

Fig. 5. Spectral characterization data processing diagram.

To derive the camera's SRF, it is necessary to observe the digital response of the camera for each wavelength emitted by the monochromator and compare it to the response of the reference detector. The camera was mounted in an integrating sphere positioned at the output of the monochromator. This sphere ensures the radiation reaches the camera sensor as homogeneously as possible.

The function that gives camera's SRF is given by Equation (2) [12].

$$SRF_{cam}(\lambda) = \frac{DN_{cam}(\lambda) \times SRF_{det}(\lambda)}{V_{det}(\lambda) \times SRF_{cam_{max}}} \quad (2)$$

where $DN_{cam}(\lambda)$ is the mean digital numbers obtained by the camera at each wavelength, $SRF_{det}(\lambda)$ is the known response function of the reference detector, $V_{det}(\lambda)$ is the measured voltage output at each wavelength and $SRF_{cam_{max}}$ is the maximum value of the camera's SRF (used for normalization).

In order to apply the SRF in the radiometric calibration stage, a further normalization step is needed by dividing (2) by the integral of the SRF within each band, as shown in (3).

$$SRF_{norm}(\lambda) = \frac{DN_{cam}(\lambda) \times SRF_{det}(\lambda)}{V_{det}(\lambda) \times SRF_{max} \times \int_{\lambda_1}^{\lambda_2} SRF_{cam}(\lambda) d\lambda} \quad (3)$$

Manual camera settings ISO and exposure times were used. Table II shows the selected configurations designed to optimize sensitivity due to low light intensity output provided by the monochromator, avoiding loss of data [13], while maintaining high digital numbers response in the central wavelengths for each band.

TABLE II. CAMERA SETUP FOR SPECTRAL CHARACTERIZATION.

Sensor	ISO	Exposure time (µs)
Green	6.378	5.988
Red	6.378	5.988
REG	6.378	12.048
NIR	6.378	12.048
RGB	1.592	40.000

Fig. 6 presents some images samples obtained during this stage. In order to standardize the calculations and use more uniform regions in terms of DN intensity, the DN values at each wavelength consisted of the mean and standard deviation, for each sample, of the pixels within a central circle with a diameter equal to half the width of the image.

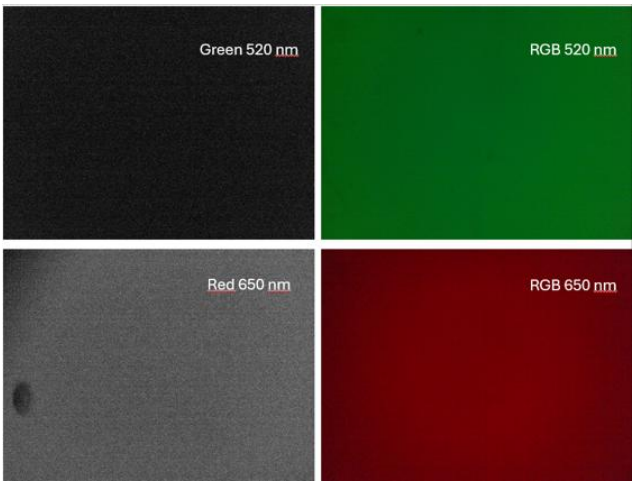

Fig. 6. Samples obtained by camera during spectral characterization phase.

V. RADIOMETRIC CALIBRATION

Following the SRF acquisition, the next step is radiometric calibration. The objective here is to determine the relationship between the mean Digital Numbers (DN) of image pixels and the radiance reaching the camera sensors.

In the first step, the radiance values emitted by the Integrating Sphere were measured using the FieldSpec 4 spectroradiometer (see Fig. 4). In the second step, images were acquired with the Parrot Sequoia camera positioned at the same location as the FieldSpec 4, at 41.4 cm from the sphere's output (Fig. 7). An environmental parameter sensor monitored air temperature, pressure, and relative humidity to ensure these conditions remained stable during the measurements, preventing undesirable bias in the results.

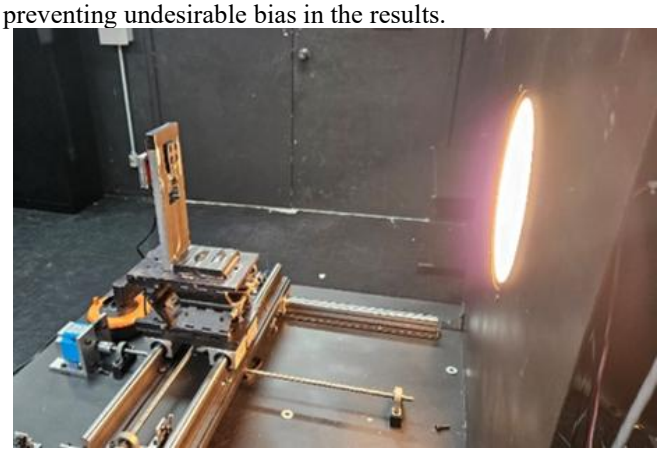

Fig. 7. Experimental setup for image capturing from integrating sphere with the Sequoia Parrot Camera.

Fig. 8 illustrates the data processing workflow performed in this stage, with the main equipment used shown in light orange fields. The numbers in red represent the key data generated, following the same sequence previously employed in the spectral characterization phase, shown in Fig. 5. $DN\ (Pot)$ refers to the DNs produced by the camera for each power level emitted by the integrating sphere, $l\ (\lambda, Pot)$ denotes the spectral radiance obtained by the FieldSpec 4, as well as $\sigma\ (\lambda, Pot)$ refers to standard deviation from data. The normalized SRF from the previous step is used here as SRF_{norm_λ}. $L_{\lambda,Pot}$ represents the effective radiance received by the sensor after multiplying data by SRF, and $L_{B,Pot}$ is the total band radiance obtained by integrating within the band limits.

A linear relationship between $DN\ (Pot)$ and $L_{B,Pot}$ was established for each power level that did not saturate the image. The least-squares method (LSM) was used to fit the calibration curve and define its coefficients.

The FieldSpec 4 provides radiance data in W/sr·m²·nm. For each power setting on integrating sphere, ten spectral radiance measurements were collected, from which the average and standard deviation were computed. Fig. 9 displays the spectral radiance curves for the 11 power combinations from 350 nm to 2500 nm.

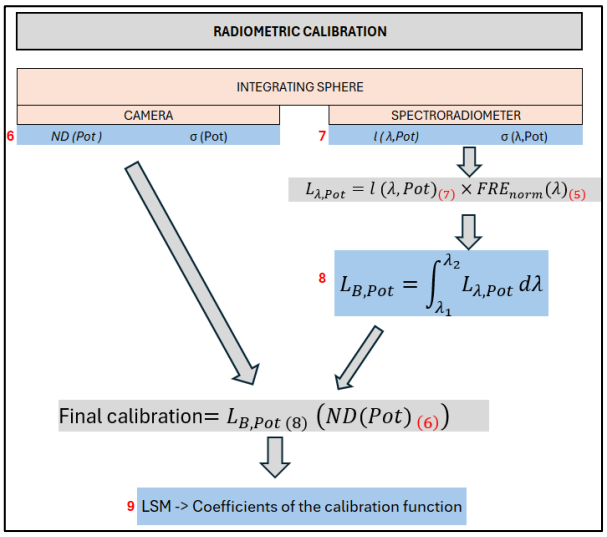

Fig. 8. Radiometric calibration workflow.

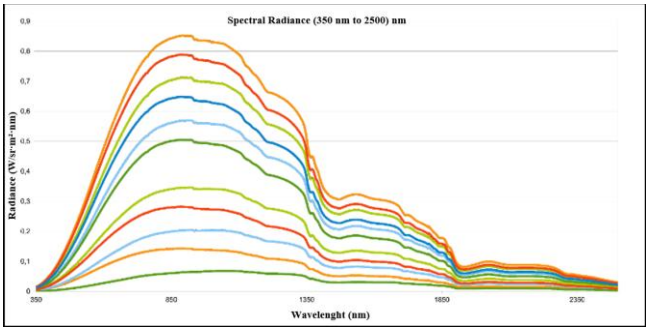

Fig. 9. Spectral radiance for 11 power combinations from integrating sphere.

After obtaining the spectral radiance correspondent to each power output, radiance that reaches each camera sensors is calculated by multiplying radiance and SRF normalized on each sensor, defined by (4).

$$L_{\lambda,Pot} = l\,(\lambda, Pot) \times SRF_{norm_\lambda}, \qquad (4)$$

where $L_{\lambda,Pot}$ is spectral radiance (with its SRF applied), $l\,(\lambda, Pot)$ is spectral radiance obtained by spectroradiometer and FRE_{norm_λ} is the normalized SRF on each camera sensor.

Then, the total radiance in the band of interest was calculated by integrating $L_{\lambda,Pot}$ over the wavelength interval, shown in (5).

$$L_{B,Pot} = \int_{\lambda_1}^{\lambda_2} L_{\lambda,Pot}\, d\lambda \qquad (5)$$

$L_{B,Pot}$ will be used on the last phase of calibration. The integration limits were 500–850 nm for the monochromatic sensors and 400–850 nm for the RGB sensor.

Subsequently, the Sequoia camera was positioned in front of the Integrating Sphere to capture images using all five of its sensors, under the eleven different power settings. The images were acquired in manual mode, with the configurations described in Table III.

TABLE III. RADIOMETRIC CALIBRATION SETUP.

Sensor	ISO	Exposure time (µs)
Green	100	30
Red	100	30
REG	100	230
NIR	100	30
RGB	100	200

The calculation of the mean DN values for each image was performed by extracting a central circular region with a diameter of 250 pixels for the monochromatic sensors and 900 pixels for the RGB sensor, corresponding to approximately 27% of the original illuminated circular area. This image cropping and the calculation of the mean and standard deviation of the DNs were carried out using the ImageJ software.

The selected settings aimed to maximize the use of the camera's dynamic range without any loss of information, meaning the DN values were close to the maximum at higher power levels but still below saturation, as exemplified in Fig. 10, which shows the circular crop performed on the REG sensor image with only the 150 W lamp turned on, along with the corresponding histogram of DN value distribution.

Finally, the obtained mean and standard deviation DN data were used to perform the final calibration in conjunction with the radiance data, resulting in the relationship between Radiance and Digital Numbers, $L_{B,Pot}$ (DN_{Pot}).

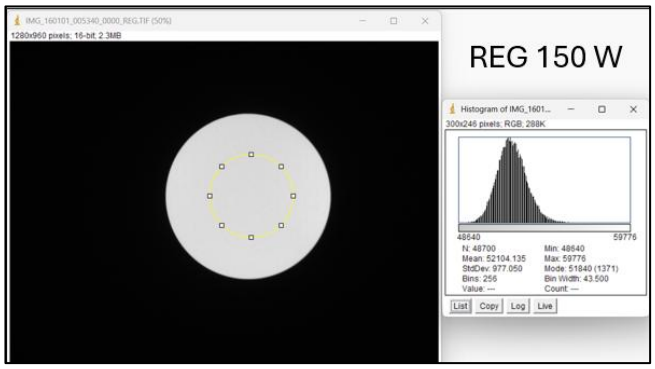

Fig. 10. Image sample obtained on integrating sphere, with the extracted central circular region, and the DN distribution histogram.

VI. RESULTS AND CONCLUSIONS

The proposed methodology enabled the spectral and radiometric calibration of the Parrot Sequoia camera.

Fig. 11 and 12 present the SRF of the monochromatic and RGB sensors, respectively. The results are consistent with manufacturer data from Table I.

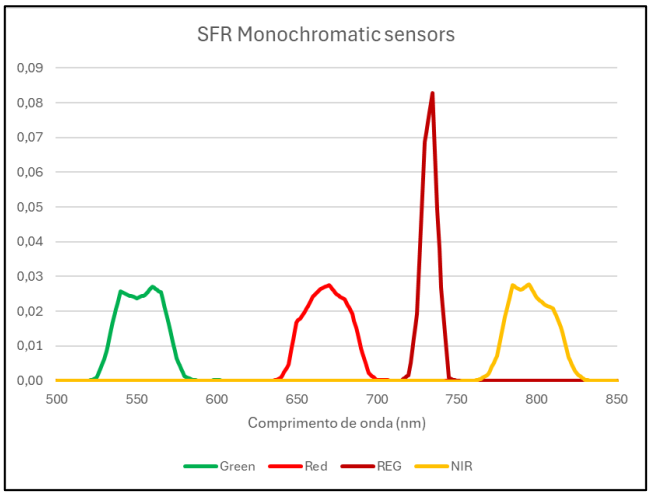

Fig. 11. Sequoia monochromatic sensors SRF.

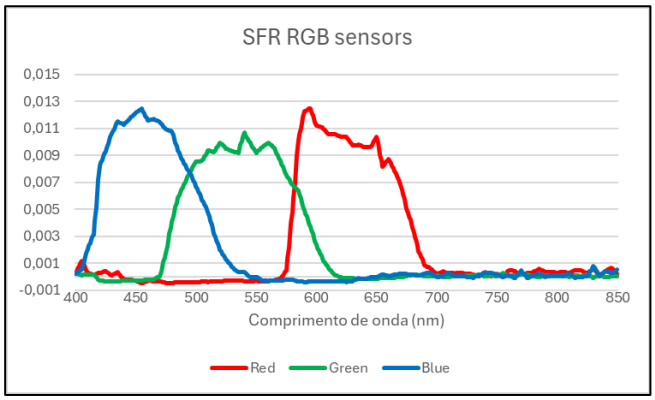

Fig. 12. Sequoia RGB sensors SRF.

Fig. 13 shows the radiometric calibration curves and coefficients for monochromatic sensors. Only six data points were used due to saturation in the higher power settings.

The linearity observed in the plots confirms that a straight line can accurately model the DN-to-radiance relationship for the monochromatic sensors, allowing the determination of calibration coefficients.

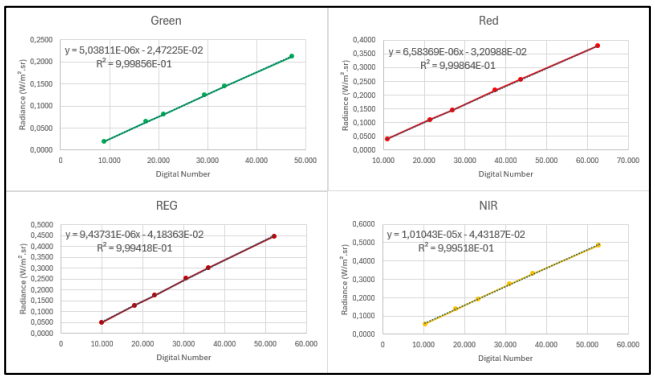

Fig. 13. Monochromatic sensors calibration.

This methodology is replicable and applicable to pre-launch calibration of any electro-optical imaging sensor used in orbital remote sensing missions.

REFERENCES

[1] BRAZIL. Air Force Command. Ordinance No. 1.225/GC-3, Nov 10, 2020. Approves the Basic Doctrine of the Brazilian Air Force (DCA 1-1), Vol. 2.

[2] Pinto, C. et al., "First in-flight radiometric calibration of MUX and WFI on-board CBERS-4," *Remote Sens.*, vol. 8, no. 5, 2016. doi: 10.3390/rs8050405.

[3] Costa, M. V. Q. S. A., Damião, A. J., Castro, R. M., "Study of radiometric calibration methods for orbital optical sensors," *SIGE 2023*. https://www.sige.ita.br/edicoes-anteriores/2023/st/235420_1.pdf

[4] Ponzoni, F. J. et al., *Calibração de Sensores Orbitais*, São Paulo: Oficina de Textos, 2015.

[5] Pinto, C. T. et al., "Evaluation of uncertainty in spectral band adjustment factor (SBAF) for cross-calibration using Monte Carlo simulation," *Remote Sensing Letters*, vol. 7, no. 9, pp. 837–846, Sep. 2016. doi: 10.1080/2150704X.2016.1190474.

[6] Parrot, *Parrot Sequoia User Guide*, v1.1, May 2017. https://www.parrot.com/assets/s3fs-public/2021-09/sequoia-userguide-en.pdf

[7] Franzini, M. et al., "Geometric and radiometric consistency of Parrot Sequoia multispectral imagery for precision agriculture," *Applied Sciences*, vol. 9, no. 24, Dec. 2019. doi: 10.3390/app9245314.

[8] Santos, J. et al., "Image saturation assessment for spatial characterization of electro-optical imaging sensors." https://proceedings.science/p/164408

[9] Acton Research Corporation, *Spectrapro-2500i Operating Instructions*, 2003.

[10] Labsphere, *Uniform Source System USS-2000 Manual*, Rev 3.

[11] ASD Inc., *FieldSpec 4 User Manual*, Document 600979, Rev F, May 2016.

[12] Lima Filho, G. M., "Methodology for the characterization of electro-optical systems for maritime patrol missions," Master's Thesis, ITA, 2015.

[13] Hiscocks, P. D., "Measuring Luminance with a Digital Camera," 2011. https://www.atecorp.com/atecorp/media/pdfs/data-sheets/Tektronix-J16_Application.pdf